01 Jul 1999

Comparative Hydrodynamics Study in a Bubble Column using Computer-Automated Radioactive Particle Tracking (CARPT)/computed Tomography (CT) and Particle Image Velocimetry (PIV)

Jinwen Chen

Abdenour Kemoun

Muthanna H. Al-Dahhan
Missouri University of Science and Technology, aldahhanm@mst.edu

Milorad P. Duduković

et. al. For a complete list of authors, see https://scholarsmine.mst.edu/che_bioeng_facwork/1376

Recommended Citation

J. Chen et al., "Comparative Hydrodynamics Study in a Bubble Column using Computer-Automated Radioactive Particle Tracking (CARPT)/computed Tomography (CT) and Particle Image Velocimetry (PIV)," *Chemical Engineering Science*, vol. 54, no. 13 thru 14, pp. 2199 - 2207, Elsevier, Jul 1999.
The definitive version is available at https://doi.org/10.1016/S0009-2509(98)00349-2

PERGAMON

Chemical Engineering Science 54 (1999) 2199–2207

Chemical Engineering Science

Comparative hydrodynamics study in a bubble column using computer-automated radioactive particle tracking (CARPT)/computed tomography (CT) and particle image velocimetry (PIV)[1]

Jinwen Chen[a], Abdenour Kemoun[a], Muthanna H. Al-Dahhan[a,*], Milorad P. Dudukovi[a], D.J. Lee[b], Liang-Shih Fan[b]

[a] *Chemical Reaction Engineering Laboratory, Washington University in St. Louis, One Brookings Drive, St. Louis, MO 63130, USA*
[b] *Department of Chemical Engineering, The Ohio State University, 140 West 19th Avenue, Columbus, OH 43210, USA*

Abstract

The hydrodynamics of a 10-cm-diameter cylindrical bubble column at the superficial gas velocity of 2, 4, and 8 cm/s are investigated by computer-automated radioactive particle tracking (CARPT), particle image velocimetry (PIV), and computed tomography (CT). These experimental techniques are capable of providing the knowledge of velocity and holdup fields in a bubble column system, which are essential as the experimental benchmark for modeling of such systems. The flow field of liquid phase, as well as the Reynolds stresses, obtained by CARPT and PIV in an air–water system are compared in detail. The results indicate that CARPT and PIV complement each other well. Further, the profile of gas holdup obtained by gamma ray based on CT compares favorably to the independently determined holdup.

Keywords: Bubble columns; CARPT; CT; PIV; Normal stress; Shear stress

1. Introduction

Bubble column reactors are used in diverse applications such as absorption, catalytic reaction, bioreaction, and coal liquefaction (Fan, 1989). The hydrodynamics in bubble columns have been extensively studied over the past few decades. In recent years, the development of advanced instrumentation techniques enlightened the experimental quantification of local and overall global flow patterns including time averaged axial and radial velocities, as well as of turbulent parameters, and phase distributions. Many advanced techniques and methods have been reported for probing the details of the flow field in bubble column systems. Among such advanced techniques, computer automated radioactive particle tracking (CARPT) (Devanathan et al., 1990; Moslemian et al., 1992; Yang et al., 1993; Degaleesan, 1997), computed tomography (CT) (Kumar, 1994; Kumar et al., 1995, 1997), particle image velocimetry, (PIV) (Chen and Fan, 1992; Reese et al., 1993; Chen et al., 1994; Hassan et al., 1998), hot-film anemometry (HFA) (Franz et al., 1984; Menzel et al., 1990), and laser doppler anemometry (LDA) (Franz et al., 1984; Groen et al., 1996; Mudde et al., 1997a) have shown their capability of exploring multiphase flow systems.

The non-invasive CARPT and CT techniques have been successfully used to measure velocities, turbulent parameters, and holdup distributions throughout the column in multiphase systems (Larachi et al., 1997). Especially, the CARPT and CT techniques are uniquely suited for opaque systems, i.e. systems with large volume fraction of the dispersed phase (the gas phase in bubble columns) as well as in large diameter columns (up to 18 in so far), in which laser (or light) cannot penetrate due to

* Corresponding author. Tel.: 001-314-935-7187; fax: (314)-935-4832; e-mail: muthanna @ wuche.wustl.edu.

[1] Paper presented at the 15th International Symposium on Chemical Reaction Engineering, Newport Beach, CA, September 13–16, 1998.

0009-2509/99/$ – see front matter
PII: S0009-2509(98)00349-2

the scattering caused by bubbles. In CARPT, to investigate the liquid flow, the instantaneous position of a single radioactive particle, which is neutrally buoyant, is continuously monitored with the help of up to 32 scintillation detectors around the column. Furthermore, the solids motion in a multiphase system can be studied by matching the size and density of the radioactive particle with solid particles. Using the CARPT technique, Lin et al. (1985) were able to study the solids motion in a gas–solid fluidized bed. The liquid motion in gas–liquid bubble columns has been investigated by Devanathan et al. (1990), Moslemian et al. (1992), Yang et al. (1992), and Degaleesan (1997). Furthermore, the solids motion in liquid–solid and gas–liquid–solid fluidized beds has been determined by Limtrakul (1996) and Roy et al. (1997) with the help of the CARPT technique. The CARPT technique provides Lagrangian information throughout the column.

Computed tomography (CT), in the Chemical Reaction Engineering Laboratory (CREL) at Washington University, relies on a hard encapsulated gamma ray source (100 mCi ^{137}Cs source), and a fan beam of collimated sodium iodide detectors to obtain projections across an entire cross-section of the column. The inversion of the scan produces a time-averaged holdup distribution over the cross-section.

The non-invasive PIV technique has the ability to quantify the instantaneous flow field, as well as the time-averaged flow patterns (Chen and Fan, 1992; Chen et al., 1994; Mudde et al., 1997b) in selected planes of the column. It can also assess the coupling effects of the flow field that may be lost when using point measurement techniques. Chen et al. (1994) studied the instantaneous flow phenomena of a bubble column using flow visualization and the PIV system. Through the use of the PIV system, they demonstrated that the averaged flow field could not represent the instantaneous macroscopic phenomena, such as "swirling" or "swing" motion when the flow information was averaged. Mudde et al. (1997b) studied the hydrodynamics of 2-D bubble columns. The velocity and Reynolds stress profiles were obtained and discussed in relation to large-scale structures present in the flow, such as the vortical structure and the structure of the fast bubble flow region.

In this study, the flow information of a 10.2 cm bubble column in both temporal and spatial scales is obtained by the two techniques, CARPT and PIV, in independent experiments, and the results are compared in detail. The same configuration of the bubble column and the same operating conditions are used in the independent experiments. Such a comparative study is necessary to verify the techniques and provide quantitative information on the fluid dynamics of bubble column systems. Furthermore, reliable hydrodynamic information is essential for development and verification of computational fluid dynamics model.

2. Experimental

2.1. Experimental conditions

The same configuration of bubble column and the same operating conditions are used in the CARPT, PIV, and CT experiments. A cylindrical column is made of Plexiglas and the dimension of the column is 10.2 cm inner diameter and 180 cm height. Compressed air and tap water is used as the gas and liquid phases, respectively. It should be noted that the tap water used in the two experiments is not quite the same in terms of the contents of impurities and surfactants. The liquid phase is operated under batch conditions, and the static liquid height is kept constant at 130 cm. The flow rate of compressed air is measured by a rotameter. A perforated plate is located between the bottom flange of the column and the plenum. The gas phase is distributed into the column by the perforated plate with 94 holes of 0.5 mm in diameter, which yields the opening area of 0.23%. The superficial gas velocities of 1.9, 4.0, and 8.0 cm/s measured at ambient condition are used in this study.

2.2. CARPT facility

Details about the software and hardware used for CARPT can be found in Devanathan (1991). In this study, a number of radioactive Scandium-46 (^{46}Sc) particles of 0.02 mm diameter and 2.89 g/cm^3 density emitting gamma rays of constant energy at 0.89 and 1.12 MeV are embedded into a polypropylene particle with a diameter of about 2.38 mm. The total strength of the radioactive particles is about 200 μCi. In order to match the density of the liquid phase, an air void is created inside the polypropylene particle (a hole of 2 mm diameter and 2 mm depth is made inside the polypropylene particle) so that the density of the composite (scandium–polypropylene–air) is equal to the density of the liquid phase being tracked.

The intensity of the gamma rays emitted by the tracer particle is continuously monitored by an array of 24 NaI (Tl) scintillation detectors of 5 cm diameter, which are strategically located around the column. To determine the exact position of the tracer particle at each instant in time, calibrations are performed for each detector, providing a relationship between the distance from the detector to the particle and the intensity count received by the detector. Using the calibration information and the intensities of radiation received by detectors at each sampling period (sampling frequency = 50 Hz), the instantaneous position of the particle is calculated. For calculation purposes, the whole column is divided into fictitious cells. An instantaneous velocity is obtained by time differentiation of particle position data and is assigned to a cell that contains the mean particle position between two successive locations. Ensemble-averaged

velocities and other turbulence quantities are calculated for all column locations upon running the experiment for over 20 h. The accuracy of the CARPT technique is described by Degaleesan (1997) and Larachi et al. (1997).

2.3. CT scanner

The CT scanner in CREL uses the third-generation fan-beam scanning configuration. The details of the hardware and software have been described in Kumar (1994) and Kumar et al. (1995, 1997). The configuration of the scanner consists of an array of NaI (Tl) detectors of 5 cm diameter (three detectors are used for the present study), and an encapsulated 100 mCi ^{137}Cs source located opposite to the center of the array of detectors. The detectors and the source are mounted on a plate, which can be rotated around the axis of the column by a step motor controlled through a microprocessor. Moreover, the whole assembly can be moved up and down along the column to scan different axial levels of the column. The source collimator provides a fan beam of 40° in a horizontal plane. There are rectangular holes of 0.5×1.0 cm at locations appropriate to each of the detectors for sampling the beams. The dimensions of the collimator are optimized based on considerations for providing adequate areas for detecting photons with good statistics in the chosen sampling time (Kumar, 1994). This design of the CT scanner yields a spatial resolution of 0.35 and 1 cm in horizontal and vertical directions, respectively.

2.4. PIV facility

A high-resolution (512×480 pixels) and high-framing rate (240 fields per second) CCD (charge-coupled device) equipped with a variable electronic shutter ranging from 1/60 to 1/20000 s is used to record the image of the flow field. The flow field is illuminated by a laser sheeting technique. A 4W argon ion laser system is used as the laser source, which is operated in a continuous mode, and a laser sheet of 3–5 mm thickness is created through the use of a cylindrical lens. A high-capacity (256 MB on-board memory) frame grabber with 40 MHz pixel clock is used to digitize the analog output from the high-resolution/high-framing rate CCD array. The high-framing rate camera is also connected to the high-speed video recorder to store the images for further studies.

The image processing occurs in five steps: (1) image acquisition, (2) image enhancement, (3) particle identification and calculation of the centroids, (4) discrimination of the particle images between the two phases, and (5) matching of the particles in three consecutive video fields and calculation of the velocity. The PIV technique used here operates at low seeding densities (typically a few particles per cm^2 viewed), and utilizes a particle-tracking algorithm to determine the velocity fields. Additional details regarding the PIV setup and data processing can be found elsewhere (Chen and Fan, 1992; Chen et al., 1994).

3. Results and discussion

3.1. Typical results obtained by CARPT and CT

As already mentioned, from the CARPT experiments, ensemble-averaged liquid recirculation velocities and turbulence quantities can be calculated for all column locations in a bubble column. Fig. 1 displays the typical results of azimuthally averaged radial profiles of the axial liquid velocity obtained from the CARPT experiments at the axial level between 72 and 82 cm from the distributor. It is clear from Fig. 1 that, in the time-averaged sense, the liquid flows up in the center and flows down near the wall. This flow pattern has been observed by many investigators in bubble columns (Hills, 1974; Franz et al., 1984; Devanathan et al., 1990; Chen et al., 1994; Menzel et al., 1990; Mudde et al., 1997a). The axial velocity inversion point is at $r/R = 0.64$ for all the three superficial gas velocities.

From the CT scans, the time-averaged cross-sectional gas holdup distributions can be reconstructed at different axial locations. The radial gas holdup profiles can be calculated by azimuthal averaging. Fig. 2 shows the radial cross-sectional gas holdup distribution at an axial distance of 73.4 cm from the distributor at the superficial gas velocity of 8 cm/s. The gas holdup is high in the center and low near the column wall. The same trend was

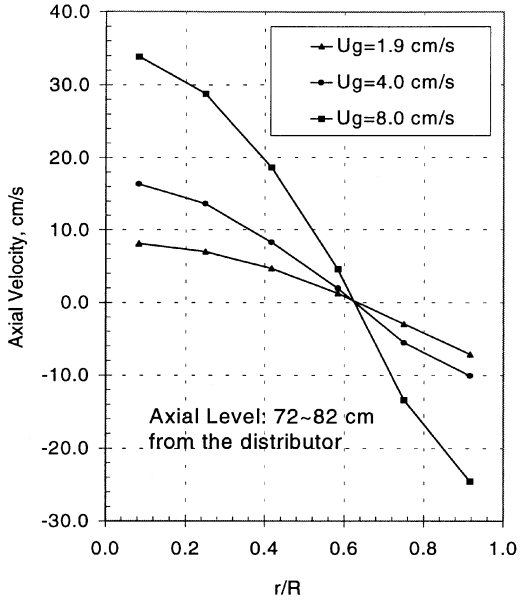

Fig. 1. Time and azimuthally averaged axial velocities obtained by CARPT.

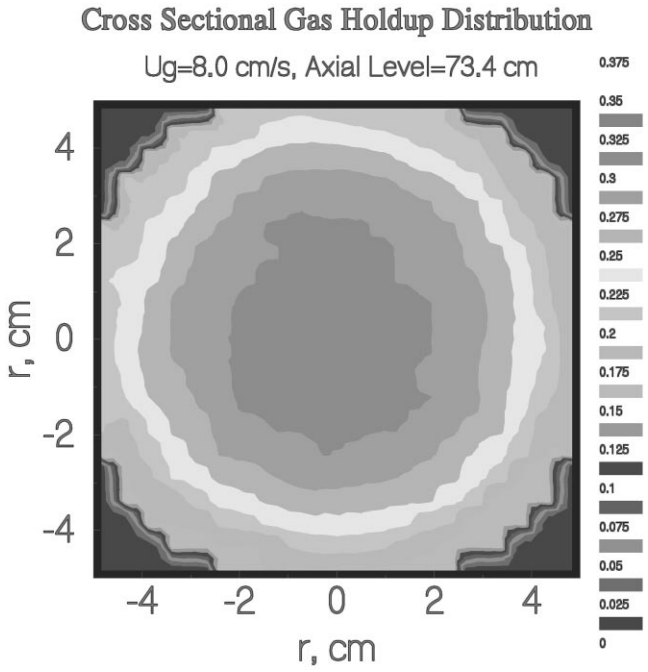

Fig. 2. Cross-sectional gas holdup distribution.

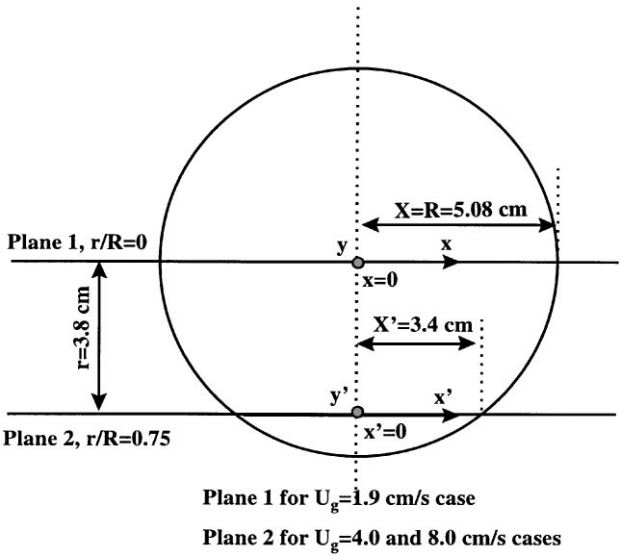

Fig. 3. Location of the laser sheet in the PIV experiments.

observed in other bubble columns of different diameters (Kumar, 1994; Kumar et al., 1995, 1996).

3.2. Typical results obtained by PIV

The positions of the laser sheet used in the PIV experiments are shown in Fig. 3. The averaged profiles of the velocity and stresses are obtained by analyzing at least 830 fields. For such a vector field, the averaged velocities are computed in vertical strips with a height equal to the field of view. The size of the field of view is 14.5 cm horizontally and 11 cm vertically at the superficial gas velocity of 1.9 cm/s, and 9.9 cm horizontally and 7.7 cm vertically at the superficial gas velocities of 4.0 and 8.0 cm/s, respectively. The averaged profiles obtained are verified to ensure that the profiles do not change significantly when the number of fields is increased. This is particularly important for the vertical velocity component. Fig. 4 shows the averaged axial, v, and radial velocity, u, profiles obtained at the gas velocity of 1.9 cm/s along Plane 1 at the axial elevation of 72.4 cm from the distributor. Note that the radial velocities are positive on left-hand side and negative on the right-hand side in the rectangular coordinate system, i.e. they are all pointing towards the center of the column. The same trend of the horizontal velocity was observed and discussed in detail by Mudde et al. (1997b). The gross scale circulation is similar to that obtained by CARPT. The profiles are the result of averaging the instantaneous swirling motion of the liquid following the central bubble stream and the related structures present in the flow.

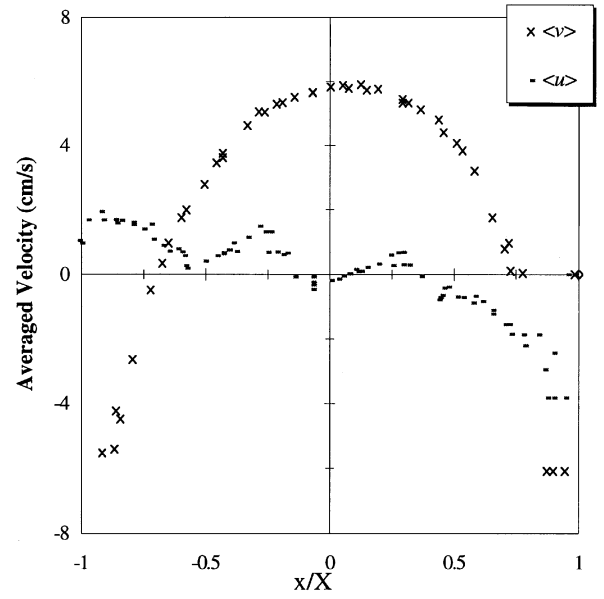

Fig. 4. Averaged velocity profiles obtained by PIV for Plane 1 at U_g = 1.9 cm/s.

For the superficial gas velocities of 4.0 and 8.0 cm/s, the data is obtained along Plane 2 and the time series of 900 consecutive vector fields are constructed for the vertical (axial) liquid velocity, v, over 9 by 7 grids. The time between two vector fields is 1/120 s. In the time series for the vertical liquid velocity, v, as shown in Fig. 5, the vortical structures are evident, i.e. periods of positive and negative axial velocity alternate. Note that Fig. 5 is obtained from the grid (4, 4) where (1, 1) represents the grid at the lower-left corner. The magnitude of velocity fluctuations increases with increased superficial gas velocity.

3.3. Comparison of CARPT/CT and PIV results

The overall gas holdups measured by the bed expansion in the PIV experiments at the superficial gas velocities of 1.9, 4.0, and 8.0 cm/s are 0.095, 0.22, and 0.30, respectively. In the CT experiments, the gas holdups corresponding to these three gas velocities are 0.083, 0.18, and 0.26, respectively. The overall gas holdups measured by the two techniques are in reasonable agreement. It is shown that the measurements in the column used in the PIV experiments show slightly higher gas holdup due to the properties of the tap water used in the two different experiments, i.e. smaller uniform bubbles are observed in the PIV experiments.

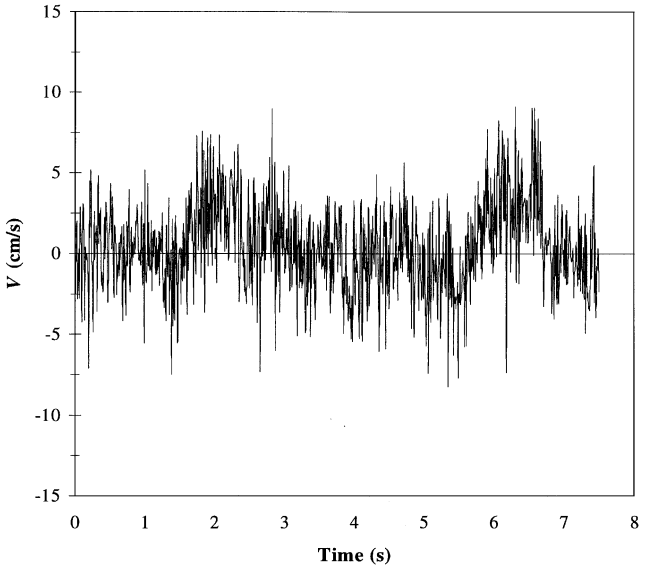

Fig. 5. Time-series of the axial velocity for Plane 2 at $U_g = 4.0$ cm/s.

At the superficial gas velocity of 1.9 cm/s, since the laser sheet in the PIV experiments is only 4 mm in thickness, the horizontal (x-direction) velocity component, u, can be taken as the radial velocity in that plane. Similarly, the axial velocity, v, measured by PIV is comparable with the axial velocity measured by CARPT in that plane. Note that the compartmentalization of the flow field for velocity calculation is different in PIV and CARPT. The top view of the compartments used in the measurement plane for PIV is shown in Fig. 6a and the side view in Fig. 6b. The top and side view of the CARPT compartments are shown in Fig. 6c and d, respectively. For the representation of measurement at Plane 1 in the PIV experiments, the shaded pie wedge shown in Fig. 6c is used in the CARPT experiments. The axial and radial velocities determined by CARPT from the pie wedge in Fig. 6c are compared with the axial and radial (x-direction) velocities of the PIV measurements at Plane 1, respectively.

At the superficial gas velocities of 4.0 and 8.0 cm/s, the laser sheet in the PIV experiments is located at $r/R = 0.75$ (Fig. 3). Note that the penetration of the laser sheet is limited by the high gas holdup, and consequently, at the superficial gas velocity of 4.0 cm/s (gas holdup = 22%) or higher, the flow field at the center of the column (Plane 1) is difficult to obtain. The velocities measured by CARPT and PIV are compared by recalculating the horizontal and vertical velocity components in CARPT. Instead of calculating r, θ, z velocity components in the cylindrical coordinates, the horizontal

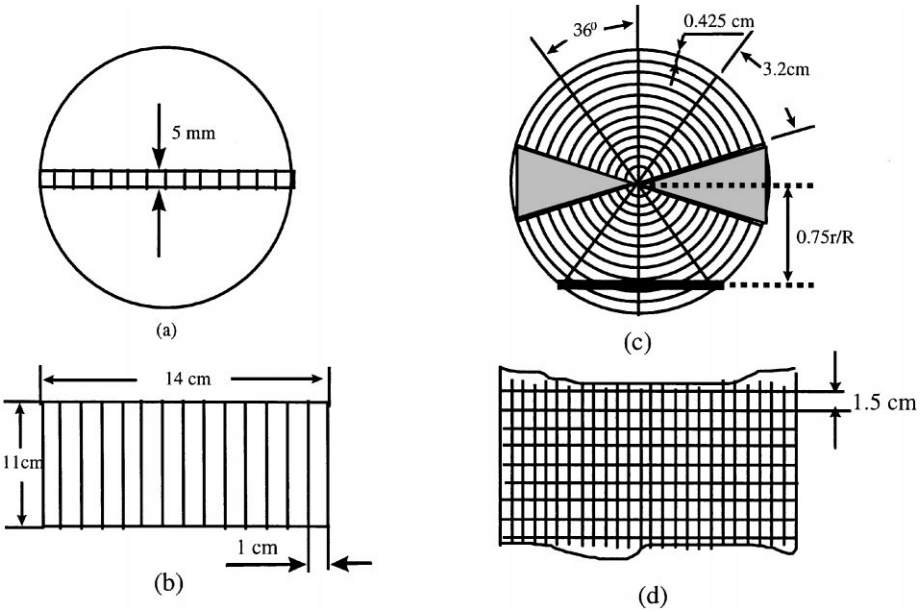

Fig. 6. Compartment configurations used in PIV (a, b) and CARPT (c, d).

(x-direction) and vertical (y-direction) velocities are obtained in the CARPT experiments. From particle trajectories in the CARPT experiments, the three velocity components (u, v, and w) can be obtained by dividing the displacements over two consecutive tracer positions in the three coordinates (Δx, Δy, and Δz) by a time step (the reverse of sampling frequency), respectively. Note that the z-direction is not the vertical direction but the direction in the horizontal plane perpendicular to the x-direction.

As mentioned earlier, CARPT collects the data over 20 h for a run. In each compartment, the tracer particle occurrence is about 400 times, leading to the particle occurrence density of 100–500 times/cm^3. The PIV results for $U_g = 1.9$ cm/s are averaged over 832 fields. The results are obtained by analyzing many sets of four consecutive fields at the sampling frequency of 240 Hz, which are randomly grabbed from the images acquired within 15 min. On the other hand, for the 4.0 and 8.0 cm/s cases, the PIV results are obtained from 1920 consecutive fields (8 s). The particle occurrence density is in the range of 20–1200 times/cm^3.

Since CARPT provides the flow pattern information in the whole column, and there are no means to identify which plane in CARPT corresponds to the plane used in the PIV experiments, an arbitrary plane (slice) is selected for this study. The choice of the plane is not essential since it is shown that the velocity profile in an arbitrary plane is not much different from the azimuthally averaged values for the whole column as shown in Fig. 7a. For comparison, a rectangular coordinate system is defined as shown in Fig. 3. Note that the y-direction represents the vertical direction.

Fig. 7a and b displays the axial, v, and the horizontal (x-direction) liquid velocity, u, at $U_g = 1.9$ and 4.0 cm/s, respectively. At $U_g = 1.9$ cm/s, the axial velocity profiles, v, measured by CARPT and PIV exhibit the same trend and the relative difference in the center of the column is about 25%. The inversion point measured by PIV seems closer to the column wall compared to that indicated by CARPT. In the CARPT experiment at the gas velocity of 1.9 cm/s, it is observed that the gas bubbles in the column are not quite uniform being larger in the top part of the column. On the other hand, in the PIV experiment, uniform and small size bubbles are observed. This may have been caused by different water impurities of the tap water used in the experiment. Slight differences that may exist in the fabrication of the two columns and distributors could also lead to the difference in bubble size distribution. In the CARPT experiment, the larger bubbles lead to the higher axial velocity of the liquid phase in the center of the column. The horizontal velocity component, u, measured by CARPT and PIV is approximately equal to one another being close to zero in the middle of the column. However, near the wall region, the PIV results show relatively high magnitude of the horizontal velocity, u, directed towards the center of the column, as discussed previously.

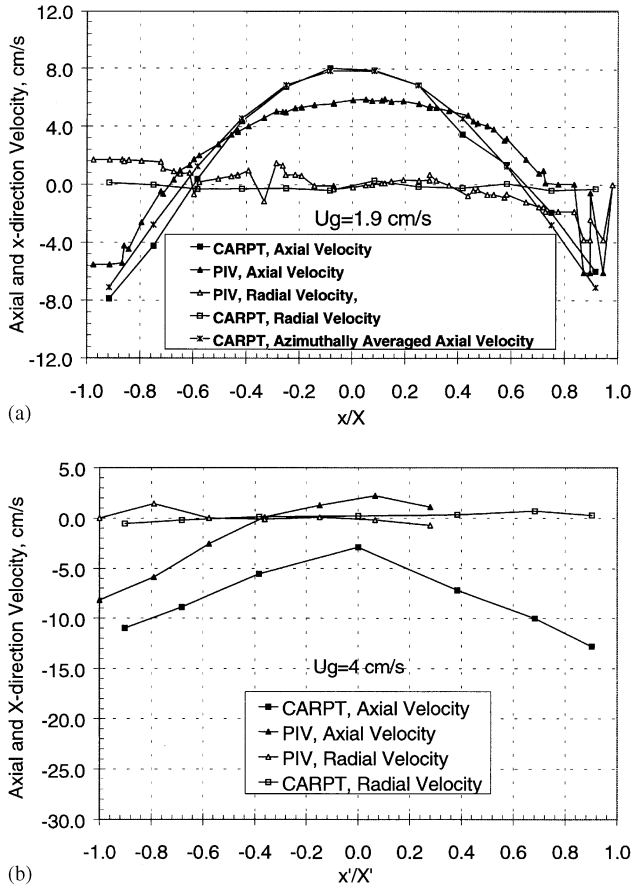

Fig. 7. Comparison of axial and radial velocities obtained by CARPT and PIV (a) for Plane 1 at $U_g = 1.9$ cm/s and (b) for Plane 2 at $U_g = 4.0$ cm/s.

The axial velocity determined by CARPT encompasses a symmetric profile as evident from Fig. 7a. The velocities measured by CARPT are obtained from a relatively larger slice of the column and with a higher number of tracer particle occurrences while the PIV velocity profiles are obtained by time averaging in a smaller section with a lower total number of tracer particle occurrences. Furthermore, CARPT represents a long-time averaging (over 20 h) while the PIV information is obtained by averaging over relatively shorter time periods, 15 min at $U_g = 1.9$ cm/s and 8 s at $U_g = 4.0$ and 8.0 cm/s.

At the superficial gas velocities of 4.0 and 8.0 cm/s, the horizontal velocities measured by both CARPT and PIV are close to zero and show no particular trend as shown in Fig. 7b. However, a relatively large difference is observed between the CARPT and PIV measured axial liquid velocities, v, although they show the same trend. The PIV result shows relatively small downward flow and detected slight upward flow near $x' = 0$. Note that Fig. 7b is obtained from the measurements at Plane 2

located at $r/R = 0.75$. The velocity profile determined by CARPT indicates a downward flow region from $r/R = 0.65$ to the column wall; hence, at $r/R = 0.75$ in the plane of measurement, the time-averaged axial velocities are directed downwards. For $U_g = 8.0$ cm/s an even larger difference in time averaged liquid axial velocity as determined by CARPT and PIV is observed. As mentioned earlier, the velocity profiles for the gas velocities of 4.0 and 8.0 cm/s cases are obtained from 8 s of consecutive images. The time-series of the axial velocity in Fig. 5 indicates a dominant frequency of 0.5 Hz. Apparently, the sampling time of 8 s is not sufficient enough to capture the ensemble time-average of the low frequency liquid flow. It should be noted that at the wall region, the profile of averaged velocity field is caused by the swirling motion of the liquid phase moving downward along the column.

In the CARPT experiments, the velocities are obtained by ensemble averaging the tracer velocity and sample all trajectories of the tracer passing through the zone of finite thickness in which velocities are recorded. In contrast, the PIV obtains the vector fields in a plane of measurement, i.e. they exclusively sample the set of trajectories that are at any time confined to the plane of measurement. Consequently, the CARPT measurement yields time-averaged velocity fields over a long-time period. On the other hand, the PIV measurement accommodates the instantaneous, full-field flow structure.

As for the Reynolds stresses, comparisons are shown in Figs. 8 and 9 at the superficial gas velocities of 1.9 and 4.0 cm/s, respectively. At $U_g = 1.9$ cm/s, as seen in Fig. 8a, the axial normal stresses measured by the two methods are of the same order of magnitude, and in the central part of the column, $-0.5 < r/R < 0.5$, reasonable agreement is observed. However, near the wall region, different trends are shown with the radial position. The axial normal stress decreases from the center to the wall for the PIV result and increases for the CARPT result. The magnitude of the radial normal stress obtained by PIV is slightly lower than that of the axial normal stress. In the CARPT measurements, the radial normal stress shows about one-third of the axial normal stress as shown in Fig. 8a. In a 60 cm diameter bubble column, Menzel et al. (1990) observed that the radial turbulence intensity is about half of the axial turbulence intensity at the superficial gas velocities of 2.4 and 7.0 cm/s. Franz et al. (1984) reported that at the superficial gas velocity of 1.2 cm/s, the radial and tangential turbulence intensities are about two-thirds of that in the axial direction. Their experiments were conducted in a 15 cm diameter bubble column with a liquid superficial velocity of 1.0 cm/s. In bubble columns, the turbulence in radial and tangential direction significantly contributes to the virtual viscosity and cannot be neglected.

Fig. 8b shows the comparison of the turbulent shear stress measured by the two techniques at $U_g = 1.9$ cm/s. Compared to the normal stresses, the shear stress is an order of magnitude lower. Fig. 8b shows that the shear stress is close to zero in the center and reaches maximum magnitude near the flow inversion point at $r/R = 0.6$. Menzel et al. (1990) reported a similar profile. They concluded that the shear stress profile is directly related to the averaged axial liquid velocity. The maximum value of the shear stress is located at the radial position of the maximum slope of the axial velocity profile. In the column center, where the averaged axial velocity is at the maximum, the shear stress is zero. A detailed analysis of the Reynolds stresses in a bubble column is discussed in Degaleesan (1997) and Mudde et al. (1997b).

At $U_g = 4.0$ cm/s, the horizontal normal stresses and the shear stress determined by PIV and CARPT are in reasonable agreement, while the PIV measurements show a relative low axial normal stress comparing with the CARPT results. The comparisons are shown in Fig. 9a and b. The lower values of axial normal stresses may be related to the lower liquid down flow detected by PIV as discussed earlier. At $U_g = 8.0$ cm/s, the results

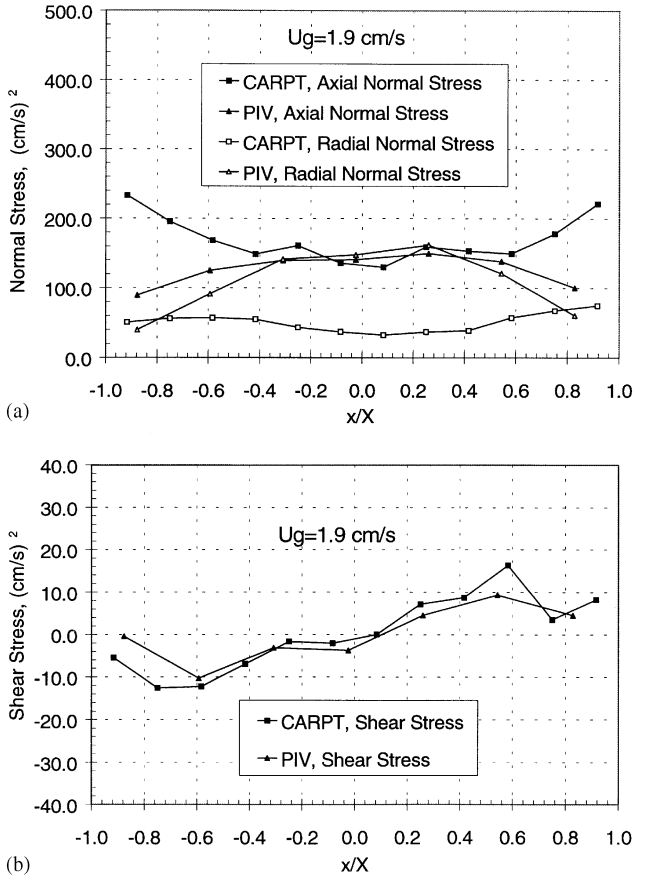

Fig. 8. Comparison of (a) the normal stresses and (b) the shear stress obtained by CARPT and PIV for Plane 1 at $U_g = 1.9$ cm/s.

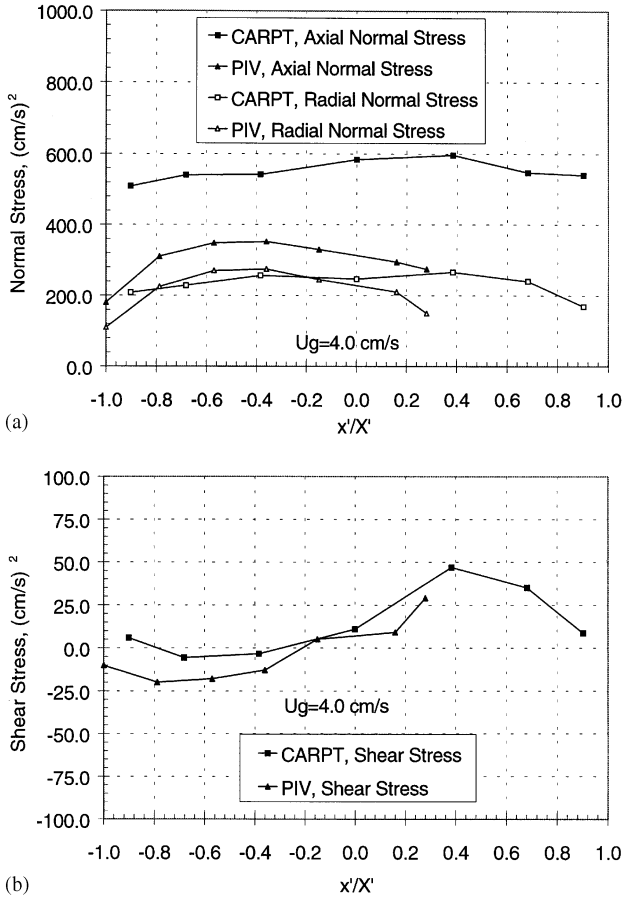

Fig. 9. Comparison of (a) the normal stresses and (b) the shear stress obtained by CARPT and PIV for Plane 2 at $U_g = 4.0$ cm/s.

follow the same trend as at $U_g = 4.0$ cm/s with slightly higher stresses, approximately 25%.

4. Concluding remarks

The velocity fields and Reynolds stresses obtained by CARPT and PIV in a 10.2 cm bubble column are compared; furthermore, the gas holdup profile is obtained by CT. The CARPT technique captures the Lagrangian description of the flow. It is shown that the CARPT technique can be used to obtain a reliable ensemble averaged quantities of the long-time behavior of liquid flow field in a bubble column. On the other hand, the PIV technique can accommodate the instantaneous, full-field flow structure of the liquid phase in a given plane; thus, the PIV system has the capability of assessing the coupling effects of the flow field. Also, the time-series information can be obtained to provide valuable characteristics of flow structure. The CARPT, PIV, and CT techniques used together can provide comprehensive insights into the complex flow structure of the turbulent two-phase flow in bubble columns.

Acknowledgements

The authors are indebted to the industrial sponsors of CREL and to Department of Energy under contract to EXXON, DOE FC 22 95 PC 95212.

Notation

r	radial position, cm
R	radius of column, cm
U_g	superficial gas velocity, cm/s
u	velocity vector in the x-direction (horizontal direction), cm/s
$\langle u'u' \rangle$	normal stress in the x-direction (horizontal direction), cm^2/s^2
$\langle u'v' \rangle$	shear stress, cm^2/s^2
v	velocity vector in the y-direction (vertical direction), cm/s
$\langle v'v' \rangle$	normal stress in the y-direction (vertical direction), cm^2/s^2
w	velocity vector in the z-direction (horizontal direction perpendicular to the x-direction), cm/s
x	horizontal coordinate, cm
y	vertical coordinate, cm
z	horizontal coordinate perpendicular to the x-direction, cm

References

Chen, R.C., & Fan, L.-S., (1992). Particle image velocimetry for characterizing the low structure in three-dimensional gas–liquid–solid fluidized beds. *Chem. Engng. Sci.*, *47*, 3615–3622.

Chen, R.C., Reese, J., & Fan, L.-S., (1994). Flow structure in a three-dimensional bubble column and three-phase fluidized bed. *A.I.Ch.E. J.*, *40*, 1093–1104.

Degaleesan, S., (1997). *Fluid dynamic measurements and modeling of liquid mixing in bubble columns*. Ph.D. thesis, Washington University in St. Louis, USA.

Devanathan, N., (1991). *Investigation of liquid hydrodynamics in bubble columns via computer automated radioactive particle tracking*. Ph.D. thesis, Washington University in St. Louis, USA.

Devanathan, N., Moslemian, D., & Duduković, M.P., (1990). Flow mapping in bubble columns using CARPT. *Chem. Engng. Sci.*, *45*, 2285–2291.

Fan, L.-S., (1989). *Gas–liquid–solid fluidization engineering*. Stoneham; MA: Butterworth.

Franz, K., Borner T., Kantorek H.J., & Buchholz, R., (1984). Flow structures in bubble columns. *Germany Chem. Engng.*, *7*, 365–374.

Groen, J.S., Oldeman, R.G.C., Mudde, R.F., & Van Den Akker, H.E.A., (1996). Coherent structure and axial dispersion in bubble column reactors. *Chem. Engng Sci.*, *51*, 2511–2520.

Hassan, Y.A., Schmidl, W. & Ortiz-Villafuerte, J. (1998). Investigation of three-dimensional two-phase flow structure in a bubbly pipe flow. *Meas. Sci. Technol.*, *9*(3), 309–326.

Hills, J.H., (1974). Radial non-uniformity of velocity and voidage in a bubble column. *Trans. Inst. Chem. Engng.*, *52*(1), 1–9.

Kumar, B.S., (1994). *Computer tomographic measurements of void fraction and modeling of the flow in bubble columns*. Ph.D. thesis, Florida Atlantic University, USA.

Kumar, B.S., Moslemian, D., & Dudukoviċ, M.P., (1995). A gamma ray tomographic scanner for imaging void fraction distribution in bubble columns. *Flow Meas. Instr*., *6*(1), 61–73.

Kumar, S.B., Moslemian, D., & Dudukovic′ M.P., (1997). Gas holdup measurements in bubble columns using computed tomography. *A.I.Ch.E. J*., *43*(6), 1414–1425.

Larachi, F., Chaouki, J., Kennedy G., & Dudukovic′, M.P., (1997). Radioactive particle tracking in multiphase reactors: Principles and applications. In: J. Chaouki, F. Larachi, & M.P. Dudukovic′ (Eds.) *Non-invasive monitoring of multiphase flows*. Amsterdam: Elsevier.

Limtrakul, S., (1996). *Hydrodynamics of liquid fluidized beds and gas–liquid fluidized beds*. Ph.D. thesis, Washington University in St. Louis, USA.

Lin, J.S., Chen, M., & Chao, B.T., (1985). A novel radioactive particle tracking facility for measurement of solids motion in gas fluidized beds. *A.I.Ch.E. J*., *31*(2), 465–473.

Menzel, T., in der Weide, T., Staudacher, O., Wein, O., & Onken, U., (1990). Reynolds shear stress for modeling of bubble column reactors. *Ind. Engng Chem. Res*., *29*(6), 988–994.

Moslemian, D., Devanathan, N., & Dudukovic′ M.P., (1992). Radioactive particle tracking technique for investigation of phase recirculation and turbulence in multiphase systems. *Rev. Sci. Instrum*., *63*(10), 4361–4372.

Mudde, R.F., Groen, J.S., & van den Akker, H.E.A., (1997a). Liquid velocity field in a bubble column: LDA experiments. *Chemical Engineering Science Proceedings of the 3rd International Conference on Gas–Liquid–Solid Reaction Engineering*, (Vol. *52*(21–22), pp. 4217–4224).

Mudde, R.F., Lee, D.J., Reese, J., & Fan, L.-S., (1997b). Role of coherent structures on Reynolds stresses in a 2-D bubble column. *A.I.Ch.E. J*., *43*, 913–926.

Reese, J., Chen, R.C., Tzeng, J.-W., & Fan, L.-S., (1993). Characterization of the macroscopic flow structure in gas–liquid and gas–liquid–solid fluidization systems using particle image velocimetry. *Int. Video J. Engng Res*., *3*, 17.

Roy, S., Chen, J., Kumar, S., Al-Dahhan, M.H., & Dudukovic′, M.P., (1997). Tomography and particle tracking studies in a liquid–solid Riser. *Ind. Engng Chem. Res*., *36*(11), 4666–4669.

Yang, Y.B., Devanathan, N., & Dudukovic′ M.P., (1993). Liquid backmixing in bubble columns via computer automated radioactive particle tracking (CARPT). *Exp. Fluids*, *16*, 1–9.